https://doi.org/10.3311/PPci.42282

Periodica Polytechnica Civil Engineering

Seismic Response Prediction of 3D Reinforcement Concrete Frames Using Machine Learning Methods

Ali Kaveh[1*], Majid Ilchi Ghazaan[1], Ali Mohammadi[1]

[1] School of Civil Engineering, Iran University of Science and Technology, P. O. B. 16765-163, Narmak, 16846-13114 Tehran, Iran
[*] Corresponding author, e-mail: alikaveh@iust.ac.ir

Received: 20 September 2025, Accepted: 23 December 2025, Published online: 28 January 2026

Abstract

This study presents a machine learning (ML) framework to forecast the nonlinear seismic behavior of three-dimensional (3D) RC moment-resisting frames, utilizing OpenSeesPy for realistic 3D modeling and nonlinear time-history analysis (NLTHA) with 110 far-field ground motions from the PEER database. A dataset of 29,700 samples was compiled, spanning 4-, 8-, and 12-story buildings with varied geometries and material properties. Seismic responses, including maximum drift, inter-story drift, and roof drift, were predicted via algorithms such as Extra Trees Regressor (ETR), Random Forest (RF), Gradient Boosting Regression (GBR), and XGBoost. Feature importance identified building height, width, Housner Intensity (HI), and Acceleration Spectrum Intensity (ASI) as key inputs. For inter-story drift, R^2 scores varied by height: for 4-story, ETR (0.9388), RF (0.9289), GBR (0.9226); for 8-story, RF (0.9833), GBR (0.9787), ETR (0.9781); for 12-story, GBR (0.9827), ETR (0.9798), RF (0.9622). For maximum drift, XGBoost achieved 0.9684, ETR 0.9678, and RF 0.9612.

Keywords

machine learning algorithm, 3D RC moment frames, nonlinear time history analysis, structural behavior, predictive model

1 Introduction

Earthquake loads are a major concern in civil and structural engineering, especially in regions prone to seismic activity. Ground motions from earthquakes generate dynamic forces that can severely damage or even collapse structures. The devastating effects consisting of loss of life, economic turmoil, and disruption to communities, highlight the critical need to accurately assess these forces and integrate them into structural design. By doing so, engineers can enhance the resilience and safety of buildings and infrastructure, particularly essential facilities like hospitals, fire stations, and emergency shelters, which must remain functional during and after seismic events. Effective earthquake load analysis not only reduces the risk of structural failure but also supports sustainable recovery by minimizing repair costs and enabling quicker rebuilding efforts [1–4].

A key part of earthquake-resistant design is accurately predicting how reinforced concrete (RC) frame structures will respond to seismic forces [5]. Modern buildings often feature complex three-dimensional (3D) RC frames, which exhibit intricate behaviors during earthquakes due to the interplay of bending, shear, and torsion, along with the nonlinear nature of materials [6, 7]. One of the most important parameters to predict is the maximum inter-story drift ratio (IDR_max), which measures the relative displacement between floors. This value correlates closely with both structural and nonstructural damage, and plays a central role in performance-based design [8–11].

Traditional seismic design often relies on simplified methods like the equivalent static force procedure, which translates dynamic earthquake forces into a set of static loads based on the building's fundamental period and mass distribution. While straightforward, this approach involves many assumptions that can lead to overly conservative designs. These compromises may hinder optimization and lead to inefficient use of materials and resources. Consequently, more precise analysis methods have emerged, offering better performance at the cost of higher computational demands [12–15].

Among these, nonlinear time-history analysis (NLTHA) is considered the gold standard for simulating how structures behave under real earthquake conditions. Using detailed finite element models—often fiber-element based—NLTHA provides highly accurate insights but requires significant

Cite this article as: Kaveh, A., Ilchi Ghazaan, M., Mohammadi, A. "Seismic Response Prediction of 3D Reinforcement Concrete Frames Using Machine Learning Methods", Periodica Polytechnica Civil Engineering, 2026. https://doi.org/10.3311/PPci.42282

computing power and long processing times, especially for tall or complex 3D RC frames. On the other hand, simplified models like lumped-mass or shear-building representations offer greater efficiency but at the cost of accuracy. This trade-off between precision and speed limits their usefulness for large-scale assessments or iterative design tasks [16–19].

To overcome these challenges, researchers are increasingly turning to machine learning (ML) techniques. These methods aim to strike a better balance between accuracy and efficiency. While simplified analytical models reduce computational time, they often fall short in capturing the nonlinear behavior of structures under seismic loads. In contrast, ML approaches have shown promising results in quickly and reliably assessing seismic damage in RC structures [20–24].

Several recent studies highlight the growing application of ML in this field. Zhang et al. [25] used a dataset of 9,900 data points generated from NLTHA of 199 RC frames under 50 different earthquakes to train random forest, XGBoost, and active learning models for rapid damage assessment. Bhatta and Dang [26] evaluated multiple ML techniques—including K-nearest neighbors, decision trees, SVMs, and neural networks—using real damage data from the 2015 Nepal earthquake. Their findings confirmed the importance of including both structural characteristics and ground motion parameters for accurate damage prediction. Similarly, Xu et al. [27] applied deep neural networks to estimate a damage index, demonstrating how ML can support broader seismic response assessments [28].

Hwang et al. [21] explored how boosting algorithms like AdaBoost and XGBoost can predict the seismic response of ductile RC frames while accounting for uncertainties in material properties—especially those affecting plastic deformation. Ahmed et al. [29] introduced a novel stacked LSTM network that used overlapping time history data to significantly reduce training time and achieve prediction accuracies of 80–95%, showing strong performance across different types of RC structures. Lazaridis et al. [30] tested ten ML algorithms to forecast damage in an 8-story RC building, identifying the best-performing model and damage index for seismic scenarios. Kaveh and Ilchi Ghazaan [31] focuses on the optimal design of three-dimensional irregular steel frames under seismic loads using response spectra, employing four metaheuristic algorithms: Colliding-Bodies Optimization (CBO), Enhanced Colliding-Bodies Optimization (ECBO), Vibrating Particles System (VPS), and a hybrid algorithm (MDVC-UVPS) combining VPS, multidesign variable configurations (MDVC), and upper-bound strategy (UBS). Frame members are selected from standard steel sections to meet practical design requirements per the LRFD-AISC code, incorporating stress, maximum lateral displacement, and geometric constraints. The hybrid MDVC-UVPS algorithm consistently outperformed CBO, ECBO, and VPS, achieving lighter designs by 4–19% across three design examples while requiring approximately 35% less computational time, demonstrating superior optimality and convergence speed. Finally, Zhang et al. [32], extended this work to damped structures, using interpretable ML models like random forest and XGBoost, as well as deep learning approaches such as convolutional neural networks and seismic wave transformers (SWT), to predict maximum inter-story displacement.

Despite these advances, important gaps remain. Most studies focus on two-dimensional (2D) models, which do not fully capture the complex 3D behavior of RC frames. Moreover, while ML methods are gaining traction, their application to 3D RC structures is still limited [33, 34]. There is also a lack of integration between data-driven ML techniques and physics-based modeling, which could improve both accuracy and interpretability. Addressing these gaps is essential to advancing the state-of-the-art in seismic response prediction for RC structures [33–35].

The aim of this research is to develop an advanced machine learning framework capable of accurately predicting the seismic response of 3D RC frames. To achieve this, we employ innovative techniques in data sampling and model optimization, including fine-tuning, halving search strategies, grid search, and k-fold cross-validation. Our dataset includes 27 unique 3D RC frame configurations—covering 4, 8, and 12-story buildings with different floor plans and heights—each subjected to 110 earthquake ground motion records. Unlike prior work focusing on 2D frames, this study prioritizes realistic 3D modeling to capture more accurate seismic behavior. The trained ML models are used to estimate key seismic parameters such as maximum drift, enabling engineers to better understand building performance, assess structural vulnerabilities, and make informed design decisions that reduce damage and improve resilience during earthquakes. Fig. 1 shows the procedure that is used in this investigation.

In this study, the structural modeling process begins with the use of ETABS software [36], where structures are analyzed using the equivalent static method to determine their final dimensions. Subsequently, the models are imported into OpenSees software [37] for three-dimensional representation. Earthquake records are then applied to the structures to extract seismic responses, generating a comprehensive dataset for further analysis.

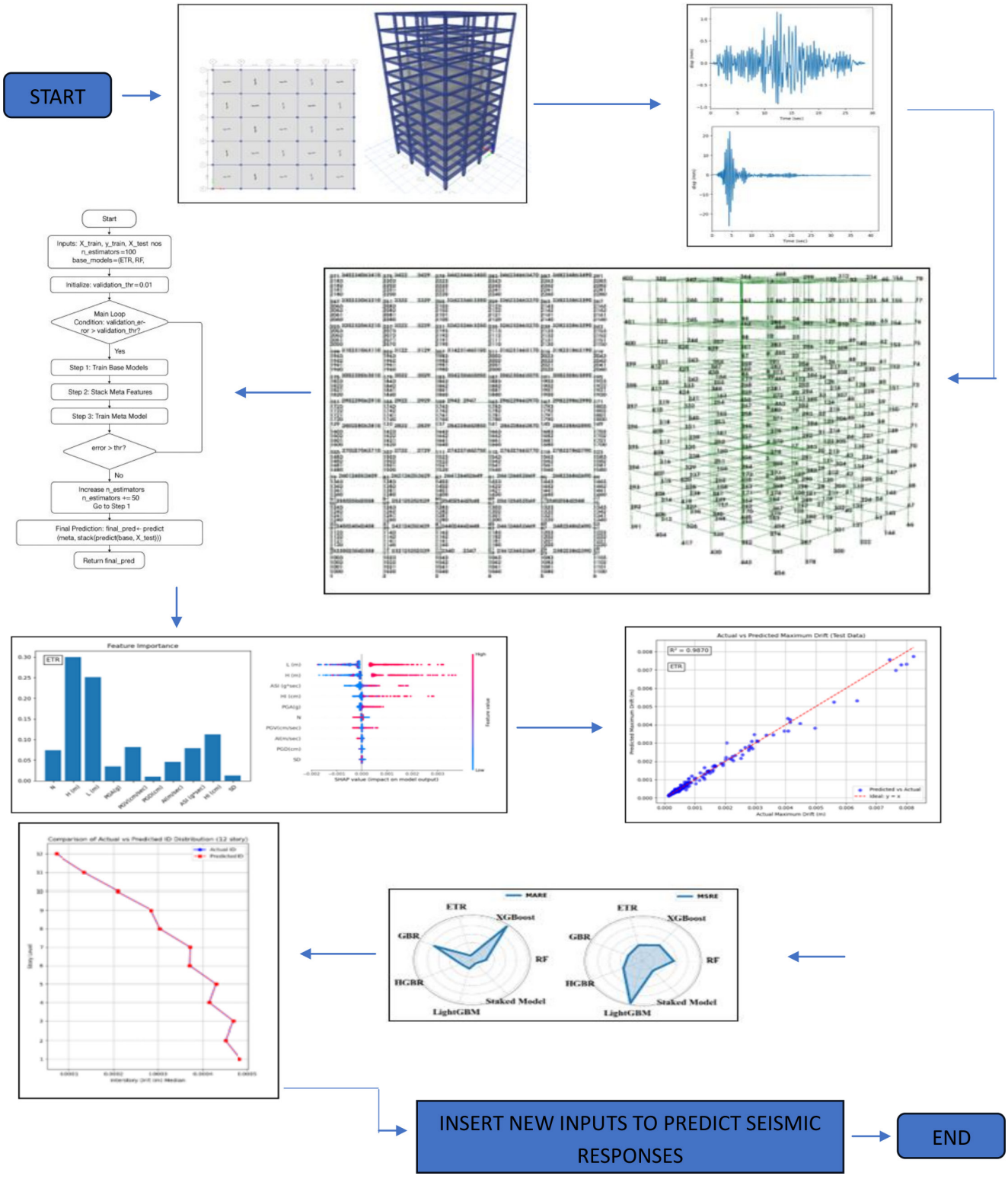

Fig. 1 Methodology workflow for NLTHA response prediction

In the next phase, machine learning techniques are employed to predict seismic responses. Multiple machine learning algorithms are utilized, and sensitivity analysis is conducted to identify optimal input parameters. The models are then trained and tested, with their performance evaluated through comparative visualizations of test results.

To assess the algorithms, six error metrics are used for comparison. A stacking algorithm, which combines multiple models, is implemented to enhance prediction accuracy. Based on the comparison, seismic responses are predicted by providing the necessary input parameters.

2 3D Reinforcement concrete frames modeling and analysis

In this study, we explored three groups of buildings with distinct floor plans based on 3 × 3, 4 × 4, and 5 × 5 grids, each featuring uniform 6-meter spans in both *X* and *Y* directions. The buildings also vary in story heights—3 meters, 3.4 meters, or 3.7 meters—to account for different design scenarios. Fig. 2 illustrates the consistent floor plans for these groups. The first group consists of 4-story buildings, the second includes 8-story buildings, and the third comprises 12-story buildings, each incorporating the three floor plan types and story height variations. All buildings use rigid connections, rigid roofs, and a reinforced concrete moment-resisting frame as the primary load-bearing system, with beams, columns, and diaphragms as key structural components.

Located in California at coordinates 37.88° N, 122.08° W, the buildings sit on Type D soil as defined by ASCE 7-16 standards [38]. The site is in a high-seismic zone, with acceleration parameters SD_1 = 0.6 g and *SDs* = 1.25 g. The design follows ASCE 7-16 [38] and ACI 318-14 [39] guidelines, using a response modification factor (*R*) of 8, a deflection amplification factor (*Cd*) of 5.5, and an overstrength factor (Ω = 3) according to ASCE 7–16 [38], ACI 318-14 [39]. For interior floors, we applied a dead load of 6 kN/m^2 and a live load of 2 kN/m^2, while the roof has a reduced dead load of 5 kN/m^2 and a live load of 1.5 kN/m^2, all compliant with ACI 318-14 requirements [39]. Fig. 3 provides 3D views of the 4, 8, and 12-story buildings with 5 × 5, 4 × 4, and 3 × 3 grids, modeled using ETABS 2016 software [36].

At the heart of structural design lies the balance between demand (the forces a structure must withstand) and capacity (its ability to resist those forces). Our goal as engineers is to ensure each element is designed with sufficient capacity to meet its demand. Initially, we considered two approaches. The first was to use a single cross-section for all beams and another for all columns, which simplifies construction and execution. However, this can be inefficient, as it does not tailor elements to their specific demands. The second approach—designing

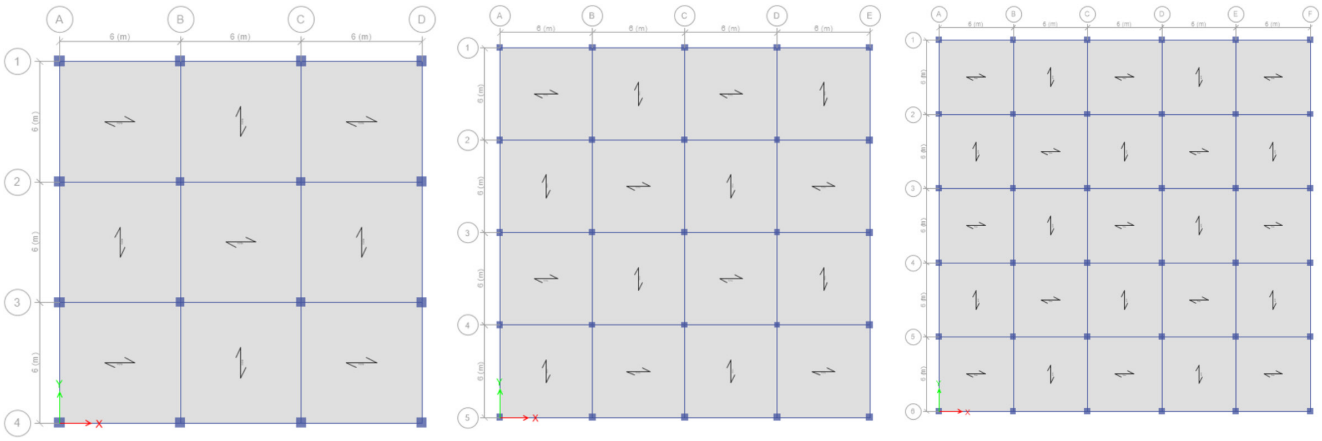

Fig. 2 Three groups of regular plans

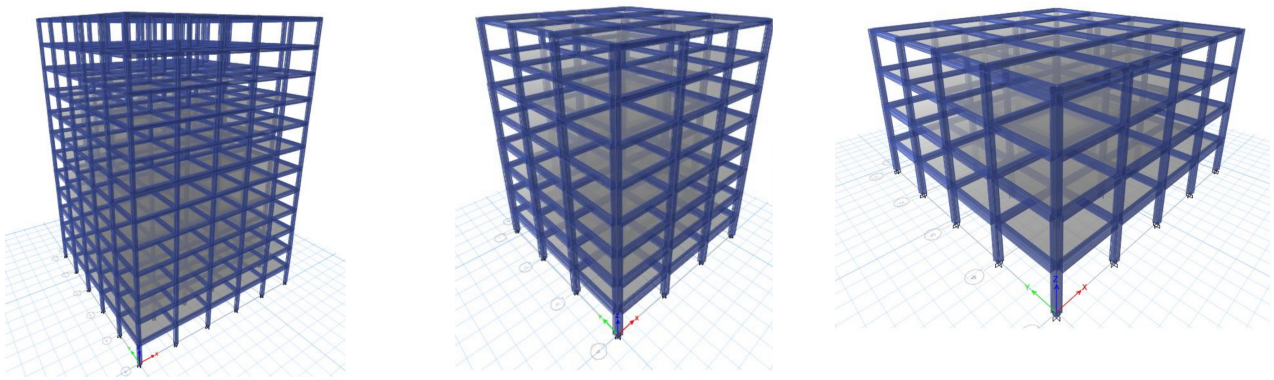

(a) (b) (c)

Fig. 3 The 3D view of the (a) 12-Story building, (b) 8-Story building, (c) 4-Story building

unique sections for every beam and column—optimizing material usage but is impractical for complex or high-rise structures due to construction challenges.

To strike a balance, we adopted a typology-based approach for beam and column design. Columns were categorized into three types based on their location: corner, edge, and interior. Beams were divided into edge and interior types. This classification remains consistent across every two floors, ensuring both constructability and cost-effectiveness.

As shown in Table 1, the 4-story buildings have 10 unique beam-column types, resulting in 90 types across the nine configurations (3 floor plans × 3 story heights). Table 2 shows that 8-story buildings have 20 types, totaling 180 across the configurations. For 12-story buildings, Table 3 indicates 30 types, leading to 270 total types. Tables 1–3 present only one representative example and that all nine plan/height combinations were analyzed, with full reinforcement details generated but omitted from the paper for saving space.

Table 1 Reinforcement details of 4 stories with a plan of 3 × 3 and a story height of 3 m

Reinforcement details of the original RC frames						
	story	Type of the element	Location	Dimension	*As* (top bars) (mm^2)	*As′* (bot. bars) (mm^2)
4 story	1&2	column	corner	500 × 500	1885	1885
			side	500 × 500	1525	1525
			middle	450 × 450	1205	1205
		beam	side	500 × 500	1500	900
			middle	450 × 450	1900	900
	3&4	column	corner	450 × 450	1700	1700
			side	450 × 450	1420	1420
			middle	400 × 400	1100	1100
		beam	side	400 × 400	1400	800
			middle	350 × 350	1250	650

Table 2 Reinforcement details of 8 stories with a plan of 3 × 3 and a story height of 3 m

Reinforcement details of the original RC frames						
	story	Type of the element	Location	Dimension	*As* (top bars) (mm^2)	*As′* (bot. bars) (mm^2)
8 story	1&2	column	corner	550 × 550	2280	2280
			side	550 × 550	1800	1800
			middle	550 × 550	2650	2650
		beam	side	500 × 500	2500	1500
			middle	500 × 500	1950	900
	3&4	column	corner	550 × 550	1800	1800
			side	550 × 550	1520	1520
			middle	550 × 550	1900	1900
		beam	side	450 × 450	2400	1700
			middle	450 × 450	1850	800
	5&6	column	corner	500 × 500	1700	1700
			side	500 × 500	1480	1480
			middle	500 × 500	1850	1850
		beam	side	400 × 400	2000	1300
			middle	400 × 400	1500	700
	7&8	column	corner	450 × 450	1200	1200
			side	450 × 450	1100	1100
			middle	450 × 450	1000	1000
		beam	side	350 × 350	1900	950
			middle	350 × 350	1400	650

Table 3 Reinforcement details of 12 stories with a plan of 3 × 3 and a story height of 3 m

Reinforcement details of the original RC frames						
	story	Type of the element	Location	Dimension	*As* (top bars) (mm^2)	*As′* (bot. bars) (mm^2)
12story	1&2	column	corner	600 × 600	2300	2300
			side	600 × 600	1900	1900
			middle	700 × 700	3600	3600
		beam	side	600 × 600	2600	1600
			middle	600 × 600	2100	1000
	3&4	column	corner	550 × 550	2250	2250
			side	550 × 550	1850	1850
			middle	700 × 700	3400	3400
		beam	side	550 × 550	2500	1800
			middle	550 × 550	2000	950
	5&6	column	corner	500 × 500	2100	2100
			side	500 × 500	1750	1750
			middle	550 × 550	3000	3000
		beam	side	500 × 500	2300	1700
			middle	500 × 500	1900	900
	7&8	column	corner	450 × 450	2000	2000
			side	450 × 450	1650	1650
			middle	450 × 450	2500	2500
		beam	side	450 × 450	2100	1500
			middle	450 × 450	1800	800
	9&10	column	corner	400 × 400	1800	1800
			side	400 × 400	1500	1500
			middle	450 × 450	2000	2000
		beam	side	400 × 400	1900	1100
			middle	400 × 400	1500	700
	11&12	column	corner	450 × 450	1500	1500
			side	450 × 450	1400	1400
			middle	450 × 450	1700	1700
		beam	side	400 × 400	1850	950
			middle	400 × 400	1400	650

We developed a detailed three-dimensional nonlinear finite element model using OpenSeesPy [37] to simulate the seismic behavior of a reinforced concrete (RC) moment-resisting frame. The prototype structure is a 12-story building with 6 bays, featuring uniform 6-meter bay spacing and a typical story height of 3.4 meters. The model uses a two-dimensional framework (*ndm* = 3) with six degrees of freedom per node (*ndf* = 6) to capture both translational and rotational behavior. RC columns and beams are modeled using force-based dispBeamColumn elements, with columns divided into 5 segments and beams into 15 segments to enhance integration accuracy and capture distributed plasticity. Material nonlinearities are represented using the Steel02 model for reinforcing steel, which accounts for isotropic strain hardening and Bauschinger effects, and the Concrete02 model for both unconfined and confined concrete. Confined concrete properties are enhanced with a 1.2 strength amplification factor to reflect transverse reinforcement effects.

Cross-sectional properties, including geometry and reinforcement layout, are defined using a fiber section approach, with data imported from a CSV file for parametric flexibility. The model incorporates varied beam and column section types to account for changes in member size and reinforcement along the building height. A PDelta transformation is applied to all elements to capture

geometric nonlinearity. Rigid beam-column connections are enforced using a custom crossJoint routine to improve convergence in joint regions. In-plane floor rigidity is simulated with rigid diaphragm constraints at each floor level, and column bases are assumed to be fixed. A concrete mass density of 2400 kg/m^3 is used to define lumped masses at nodes for dynamic analysis. The adopted confinement model influences lateral strength and ductility but does not alter the relative drift variations used for ML training, because all structural configurations follow the same confinement assumptions.

2.1 Nonlinear analysis

As discussed in the introduction, structural analysis methods fall into two broad categories: static and dynamic, each further divided into linear and nonlinear approaches. These methods, summarized in Table 4, have unique characteristics suited to different scenarios [40–42]. For this study, we opted for nonlinear time history analysis because of its superior accuracy and reliability in capturing complex structural behavior. We analyzed 110 far-field earthquake records sourced from the Pacific Earthquake Engineering Research (PEER) database, applying them to our structural models to determine the maximum drift. Since our structures are three-dimensional, we applied these earthquake records simultaneously in both the *X* and *Y* directions to reflect real-world conditions. The selected ground motions and their specific characteristics are detailed in Table 5. The selected PEER far-field records cover a wide range of intensities, including several events with very low peak ground acceleration (PGA). All records were applied at their recorded amplitudes without scaling, which preserves the natural variability in motion intensity and duration. All 110 far-field ground motions were applied in their original recorded amplitudes without scaling, in order to preserve natural variability in intensity and frequency content. This variability was intentionally retained to enhance the robustness and generalizability of the machine learning models.

Table 4 Alternative seismic analysis procedures suggested in ASCE/SEI 41-17 [40, 42]

Category	Analysis procedure	Analysis method	Seismic load
Linear	Linear static	Equivalent static analysis	Distributed static lateral load
	Linear dynamic	Response spectrum analysis/ linear dynamic analysis	Response spectrum or seismic ground motion record
Nonlinear	Nonlinear static	Pushover analysis	Response spectrum
	Nonlinear dynamic	Time history analysis	Seismic ground motion record

3 Machine learning

Machine learning (ML), a fundamental branch of artificial intelligence (AI), allows systems to learn from data and make predictions without explicit programming. ML techniques are typically classified into three categories: supervised learning (which uses labeled data for training), unsupervised learning (which focuses on discovering patterns in unlabeled data), and reinforcement learning (which learns through interaction and feedback) [43, 44].

In recent years, machine learning has become increasingly prominent across various fields, such as structural engineering (Shehzad et al. [43]), materials science and biomedicine. Each domain utilizes a range of powerful algorithms, each with its own strengths and trade-offs. These algorithms include Artificial Neural Networks (ANNs), Random Forest (RF), Extra Trees (ETR), Gradient Boosting Machine (GBM), Gradient Boosting Regression (GBR), Histogram-based Gradient Boosting Machine (HGBM), LightGBM, and XGBoost [45–47]. Modeled after the human brain, ANNs consist of layers of interconnected nodes (or neurons) capable of capturing complex, nonlinear relationships in data However, they require large datasets and considerable computational power, and can be prone to overfitting if not properly regularized ANNs have been successfully applied in areas such as surface water quality modeling rainfall forecasting and epilepsy prediction [48–50]. Gradient Boosting Machine (GBM), GBM builds models sequentially, where each new tree attempts to correct the errors of the previous one It is a robust and flexible method that handles missing data well but can be computationally intensive to train and tune effectively [46]. RF constructs a large number of decision trees during training and averages their outputs for predictions. It's relatively easy to use, resistant to overfitting, and performs well in many cases, though it may not match the predictive power of more advanced methods like GBM or XGBoost. RF has been used for predicting shear resistance of anchors olive production and groundwater classification [51–53]. Extra Trees (ETR), Similar to Random Forest, ETR adds more randomness during tree construction, which can lead to faster training and better generalization in some cases [54]. LightGBM, designed for speed and efficiency, LightGBM is a gradient boosting framework that handles large datasets

Table 5 Selected natural accelerograms

num	Earthquake name	Year	Magnitude	PGA
1	Baja California	1987	5.5	0.58026
2	Baja California	1987	5.5	0.40463
3	Baja California	1987	5.5	0.67602
4	Bam Iran	2003	6.6	0.16846
5	Bam Iran	2003	6.6	0.10926
6	Bam Iran	2003	6.6	0.08635
7	Caldiran Turkey	1976	7.3	0.05473
8	Caldiran Turkey	1976	7.3	0.06393
9	Caldiran Turkey	1976	7.3	0.09748
10	Chi-Chi Taiwan	1999	7.6	0.13738
11	Chi-Chi Taiwan	1999	7.6	0.09798
12	Chi-Chi Taiwan	1999	7.6	0.11039
13	Denali Alaska	2002	7.9	0.01225
14	Denali Alaska	2002	7.9	0.02295
15	Denali Alaska	2002	7.9	0.00763
16	El Mayor-Cucapah	2010	7.2	0.24849
17	El Mayor-Cucapah	2010	7.2	0.19699
18	El Mayor-Cucapah	2010	7.2	0.27896
19	Gulf of California	2001	6.5	0.06336
20	Gulf of California	2001	6.5	0.03835
21	Gulf of California	2001	6.5	0.00903
22	Imperial Valley-06	1979	6.4	0.03815
23	Imperial Valley-06	1979	6.4	0.11598
24	Imperial Valley-06	1979	6.4	0.12805
25	Imperial Valley-06	1979	6.4	0.11268
26	Imperial Valley-06	1979	6.4	0.20551
27	Imperial Valley-06	1979	6.4	0.16185
28	Imperial Valley-06	1979	6.4	0.04308
29	Imperial Valley-06	1979	6.4	0.05775
30	Imperial Valley-06	1979	6.4	0.02635
31	Imperial Valley-06	1979	6.4	0.1111
32	Imperial Valley-06	1979	6.4	0.20199
33	Imperial Valley-06	1979	6.4	0.08012
34	Kern County	1952	7.5	0.08969
35	Kern County	1952	7.5	0.1321
36	Kern County	1952	7.5	0.04353
37	Kobe Japan	1995	6.9	0.22063
38	Kobe Japan	1995	6.9	0.23091
39	Kobe Japan	1995	6.9	0.13841
40	Loma Prieta	1989	6.9	0.35853
41	Loma Prieta	1989	6.9	0.3266
42	Loma Prieta	1989	6.9	0.19174
43	Loma Prieta	1989	6.9	0.04887
44	Loma Prieta	1989	6.9	0.0504
45	Loma Prieta	1989	6.9	0.02757

Table 5 Selected natural accelerograms (continued)

num	Earthquake name	Year	Magnitude	PGA
46	Loma Prieta	1989	6.9	0.22466
47	Loma Prieta	1989	6.9	0.31251
48	Loma Prieta	1989	6.9	0.40607
49	Loma Prieta	1989	6.9	0.46009
50	Loma Prieta	1989	6.9	0.41676
51	Loma Prieta	1989	6.9	0.37164
52	Manjil Iran	1990	7.4	0.51456
53	Manjil Iran	1990	7.4	0.49687
54	Manjil Iran	1990	7.4	0.53804
55	Morgan Hill	1984	6.2	0.40613
56	Morgan Hill	1984	6.2	0.22289
57	Morgan Hill	1984	6.2	0.29226
58	Nenana Mountain Alaska	2002	6.7	0.01103
59	Nenana Mountain Alaska	2002	6.7	0.01087
60	Nenana Mountain Alaska	2002	6.7	0.00631
61	Northridge	1994	6.7	0.56833
62	Northridge	1994	6.7	0.51423
63	Northridge	1994	6.7	0.21734
64	Northridge	1994	6.7	0.07954
65	Northridge	1994	6.7	0.02795
66	Northridge	1994	6.7	0.04902
67	Northridge	1994	6.7	0.12612
68	Northridge	1994	6.7	0.18371
69	Northridge	1994	6.7	0.09735
70	Northridge	1994	6.7	0.0498
71	Northridge	1994	6.7	0.08892
72	Northridge	1994	6.7	0.07326
73	Northridge	1994	6.7	0.00026
74	Northridge	1994	6.7	0.08422
75	Northridge	1994	6.7	0.10588
76	Northridge	1994	6.7	0.000265
77	Northridge	1994	6.7	0.06019
78	Northridge	1994	6.7	0.03361
79	Northridge	1994	6.7	0.11573
80	Northridge	1994	6.7	0.10574
81	Northridge	1994	6.7	0.04088
82	Northridge	1994	6.7	0.10084
83	Northridge	1994	6.7	0.09496
84	Northridge	1994	6.7	0.0705
85	Northridge	1994	6.7	0.04727
86	Northridge	1994	6.7	0.05967
87	Northridge	1994	6.7	0.03427
88	Northridge	1994	6.7	0.02582
89	Northridge	1994	6.7	0.01617
90	Northridge	1994	6.7	0.00813

Table 5 Selected natural accelerograms (continued)

num	Earthquake name	Year	Magnitude	PGA
91	Northridge	1994	6.7	0.024
92	Northridge	1994	6.7	0.03253
93	Northridge	1994	6.7	0.01543
94	San Fernando	1971	6.6	0.07475
95	San Fernando	1971	6.6	0.11078
96	San Fernando	1971	6.6	0.04543
97	San Fernando	1971	6.6	0.00609
98	San Fernando	1971	6.6	0.00952
99	San Fernando	1971	6.6	0.0059
100	San Fernando	1971	6.6	0.19418
101	San Fernando	1971	6.6	0.38215
102	San Fernando	1971	6.6	0.28217
103	San Fernando	1971	6.6	0.16718
104	San Fernando	1971	6.6	0.19777
105	San Fernando	1971	6.6	0.15587
106	San Fernando	1971	6.6	0.10418
107	San Fernando	1971	6.6	0.13763
108	San Fernando	1971	6.6	0.05452
109	San Fernando	1971	6.6	0.02576
110	San Fernando	1971	6.6	0.04152

with lower memory usage. It achieves this through techniques like Gradient-based One-Side Sampling (GOSS) and Exclusive Feature Bundling (EFB). LightGBM has seen use in predicting phonon cutoff frequencies of materials and concrete strength assessment [52]. XGBoost, one of the most popular ML libraries, XGBoost offers high performance through regularization, parallel processing, and built-in handling of missing values. It's widely applied in fields ranging from medicine to cybersecurity—used, for example, in predicting glioma treatment outcomes malware detection and resume-based personality prediction [53]. Histogram-based Gradient Boosting Machine (HGBM), HGBM improves training speed and memory efficiency by binning continuous features into histograms. This makes it well-suited for large-scale data applications [46]. In the current analysis, a massive dataset of 29700 samples was used. This dataset was divided into 80% for training and 20% for testing. Hyperparameters for all models were tuned using a 5-fold cross-validation scheme applied to the training set (80% of the data). For each split, models were trained on four folds and validated on the remaining fold, and this process was repeated five times to obtain stable performance estimates. The final hyperparameters were selected based on average CV performance and the models were retrained on the full training portion. The remaining 20% of the data was kept completely unseen and was used only for final generalization assessment. By strictly separating the testing data from the training phase, the model's performance could be assessed more accurately and the risk of overfitting minimized. Ultimately, the careful selection and tuning of machine learning algorithms—combined with rigorous validation practices—are essential for building reliable, high-performing models. These models are increasingly transforming how we approach complex challenges across scientific and engineering disciplines.

3.1 Feature importance

When using machine learning to predict how buildings respond to earthquakes, we focus on a specific output, such as the maximum structural drift. However, the accuracy of these predictions heavily depends on the inputs we choose, which are often uncertain and can significantly affect the results. To build a highly accurate model, we need a method to carefully select the most relevant inputs. This is where feature importance comes in—it helps us understand how much each input influences the model's predictions.

Our model combines a structural framework with nonlinear time-history analysis, so we divided the inputs into two categories: structural inputs (related to the building's design) and seismic inputs (related to earthquake

characteristics). Initially, we considered 21 inputs but narrowed them down to 10, as shown in Fig. 4. After analyzing their feature importance, we selected three structural inputs—number of floors, total Height, and width of the structure—and seven seismic inputs: Peak Ground Acceleration (PGA), Peak Ground Velocity (PGV), Peak Ground Displacement (PGD), Arias Intensity (AI), Acceleration Spectrum Intensity (ASI), Housner Intensity (HI), and Significant Duration (SD).

Fig. 4 illustrates the feature importance for all algorithms we tested, revealing how each input impacts the model's performance. It also shows the relative importance of each input for our surrogate model algorithms using two types of visualizations: bar charts and SHAP plots. These

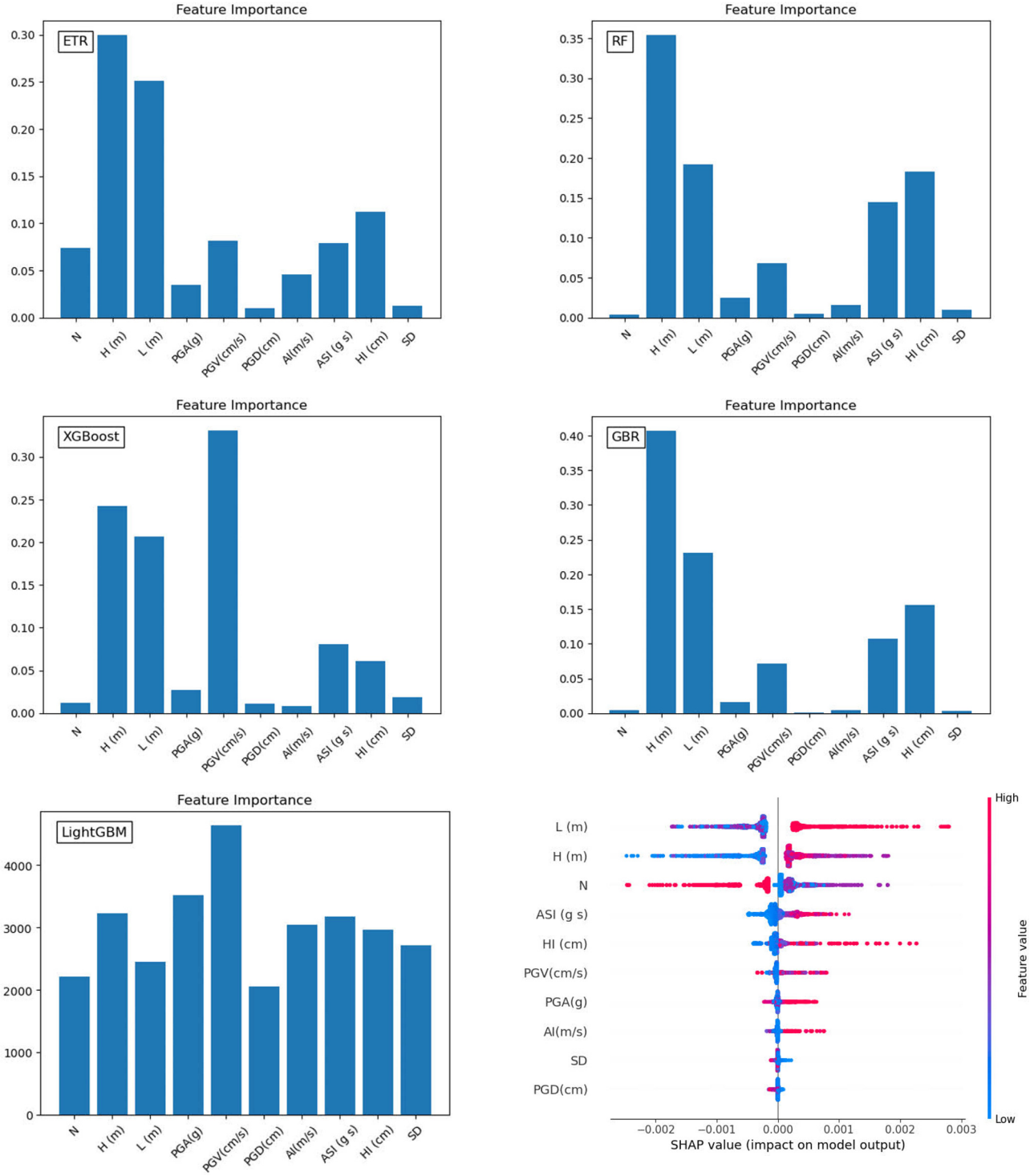

Fig. 4 Feature importance plot of input features used in the surrogate models

visuals helped us identify which inputs, when adjusted, could boost the model's accuracy. By analyzing these charts across all algorithms, we reached a clear conclusion: two structural inputs (building height) and two seismic inputs (Housner Intensity and Acceleration Spectrum Intensity) consistently stood out as critical for improving accuracy. In contrast, inputs like the number of floors, PGA, PGD, and SD had a smaller impact on the model's performance.

3.2 Stacked ML

Research on surrogate models for predicting seismic responses has shown that no single machine learning algorithm can reliably predict how structures behave under various earthquake conditions. This is understandable—earthquakes are unpredictable, and structures respond in complex ways to seismic forces. Some studies focus on developing models based on a single algorithm or improving existing ones, but these approaches often fall short. A promising solution is to combine multiple machine learning algorithms into a single framework, or "stacked model", to better estimate seismic parameters.

In this study, we set out to build a stacked model that integrates several algorithms to predict key seismic responses, such as maximum structural drift, maximum inter-story drift, and maximum roof drift. Choosing the right algorithms to include in this model is tricky. One might assume that combining all available algorithms would yield the best results, but this approach significantly increases runtime, which is a critical concern since we need a model that's both accurate and efficient.

To tackle this, we first conducted a sensitivity analysis to identify the best combination of algorithms. We started by examining the proposed machine learning models, focusing on their hyperparameters Next, we evaluated each algorithm's performance using error metrics outlined in Table 6, which helped us gauge their effectiveness. The results for these metrics, based on preprocessed datasets, are shown in Table 7, highlighting how each algorithm performed.

But we didn't stop there. To find the optimal algorithm combination for our stacked model, we analyzed various combinations and their error rates, as presented in Table 8. The results were clear: the Random Forest (RF), Gradient Boosting Regression (GBR), and Extra Trees Regressor (ETR) algorithms consistently showed higher accuracy and lower error rates compared to others (Table 7). Furthermore, Table 8 revealed that combining these three algorithms in a stacked model delivered the highest accuracy. Because several ground motions exhibit very low PGA, some analyses resulted in near-zero structural responses. Such low-demand cases are important to retain because they reflect the natural variability of seismic records; however, they can cause relative error metrics (MARE, MSRE, RMSRE) to appear large or unstable when the true response is close to zero. Therefore, absolute metrics (MAE, MSE), which remain well-behaved for very small responses, were emphasized when interpreting model performance.

Table 6 Error indicators

R-squared	$1-\frac{\sum_{i=1}^{n}\left(y_i-\widehat{y}_i\right)^2}{\sum_{i=1}^{n}\left(y_i-\overline{y}\right)^2}$
MSE	$\frac{1}{n}\sum_{i=1}^{n}\left(y_i-\widehat{y}_i\right)^2$
MAE	$\frac{1}{n}\sum_{i=1}^{n}\left\|y_i-\widehat{y}_i\right\|$
MARE	$\frac{1}{n}\sum_{i=1}^{n}\left\|\frac{y_i-\widehat{y}_i}{y_i}\right\|$
MSRE	$\frac{1}{n}\sum_{i=1}^{n}\left(\frac{y_i-\widehat{y}_i}{y_i}\right)^2$
RMSRE	$\sqrt{\frac{1}{n}\sum_{i=1}^{n}\left(\frac{y_i-\widehat{y}_i}{y_i}\right)^2}$

As a result, we used this trio—RF, GBR, and ETR—in our stacked model to predict maximum structural drift, maximum inter-story drift, and maximum roof drift. For comparison, we also tested these algorithms individually to calculate the same parameters. This approach strikes a balance between accuracy and efficiency, giving us a robust tool to predict how structures respond to earthquakes. Fig. 5 shows the flowchart of the stacked model.

4 Numerical result

After identifying the most impactful input features, we used them as variables for our machine learning (ML) algorithms. To train our predictive models, we applied data selection techniques like cross-validation to ensure robust results. For a fair comparison, all algorithms were run on a PC with an Intel Core i3-8100 CPU (3.60 GHz) and 16 GB of RAM, using Python. We selected the best-performing results from each ML algorithm for our analysis.

Our goal was to predict key seismic responses—maximum structural drift, maximum inter-story drift, and maximum roof drift—and evaluate the models' performance. No minimum-intensity threshold or filtering was

Table 7 Results of error indicators for dataset assuming ML models

ML algorithm	*R*-squared	MSE	MAE	MARE	MSRE	RMSRE
XGBoost	0.96843	7.52E-07	9.6E-05	0.167178	0.05168	0.227331
RF	0.961204	6.51E-07	8E-05	0.084174	0.029669	0.172246
ETR	0.967849	7.36E-08	7E-05	0.066811	0.013161	0.114723
LightGBM	0.911196	9.64E-07	1.25E-04	0.161752	0.149153	0.386204
GBR	0.947542	8.24E07	1.29E04	0.208762	0.112493	0.3354
HGBR	0.854468	9.58E06	1.52E04	0.193854	0.392139	0.62621
Stacked ML	0.99573	5.82E-08	5.4E05	0.060516	0.009022	0.094982

Table 8 Result of ML algorithm combination

Algorithm combination	Error	Algorithm combination	Error
RF+ETR	0.9619	RF+ETR+HGBR	0.9625
RF+HGBR	0.9607	RF+ETR+GBR	0.99573
ETR+HGBR	0.9601	ETR+HGBR+GBR	0.9708
ETR+LightGBM	0.96	ETR+HGBR+XGBoost	0.964
GBR+XGBoost	0.9437	GBR+XGBoost+LightGBM	0.9552
HGBR+XGBoost	0.94	ETR+GBR+LightGBM	0.9616

applied; all 110 ground motions were retained in the dataset to ensure unbiased representation of low-, moderate-, and high-demand conditions. Fig. 6 shows the Extra Trees Regressor (ETR) algorithm's predictions for maximum structural drift in 4-, 8-, and 12-story buildings, with impressive accuracies of 0.9678, 0.9870, and 0.9524, respectively. These results outperformed other algorithms in terms of accuracy and error rates.

While ETR excelled in predicting maximum structural drift, inter-story drift, and roof drift for 4-, 8-, and 12-story reinforced concrete buildings, other algorithms like Random Forest (RF), XGBoost, and Gradient Boosting Regressor (GBR) occasionally performed better for specific cases. Predicting the distribution of floor drift proved challenging, as no single algorithm consistently delivered accurate results across all floors. To address this, we developed a stacked model combining ETR, RF, and XGBoost, based on our sensitivity analysis. This stacked model selects the best-predicted values for each floor and plots them, leveraging parallel processing to minimize runtime while maintaining high accuracy.

Fig. 7 illustrates the predicted inter-story drift distribution for a 3D reinforced concrete structure using the stacked model with the mean method, achieving remarkable accuracies of 0.9886, 0.9862, for 4-story building, respectively. These results demonstrate the model's excellent predictive power, making it a valuable tool for structural designers. Both methods confirm the stacked model's

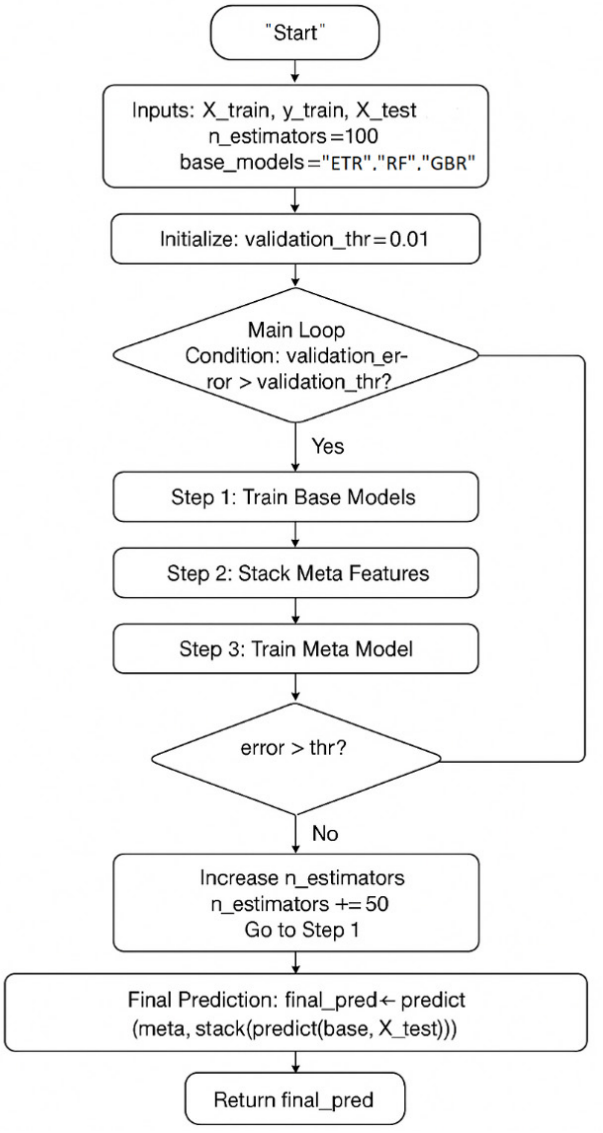

Fig. 5 Flowchart of the stacked model

versatility and reliability, with minor differences between the mean and median approaches. By predicting inter-story drift distributions, the model helps designers identify weak or soft stories, enabling proactive measures to prevent failures and streamline retrofitting for both existing and new buildings, ultimately reducing costs.

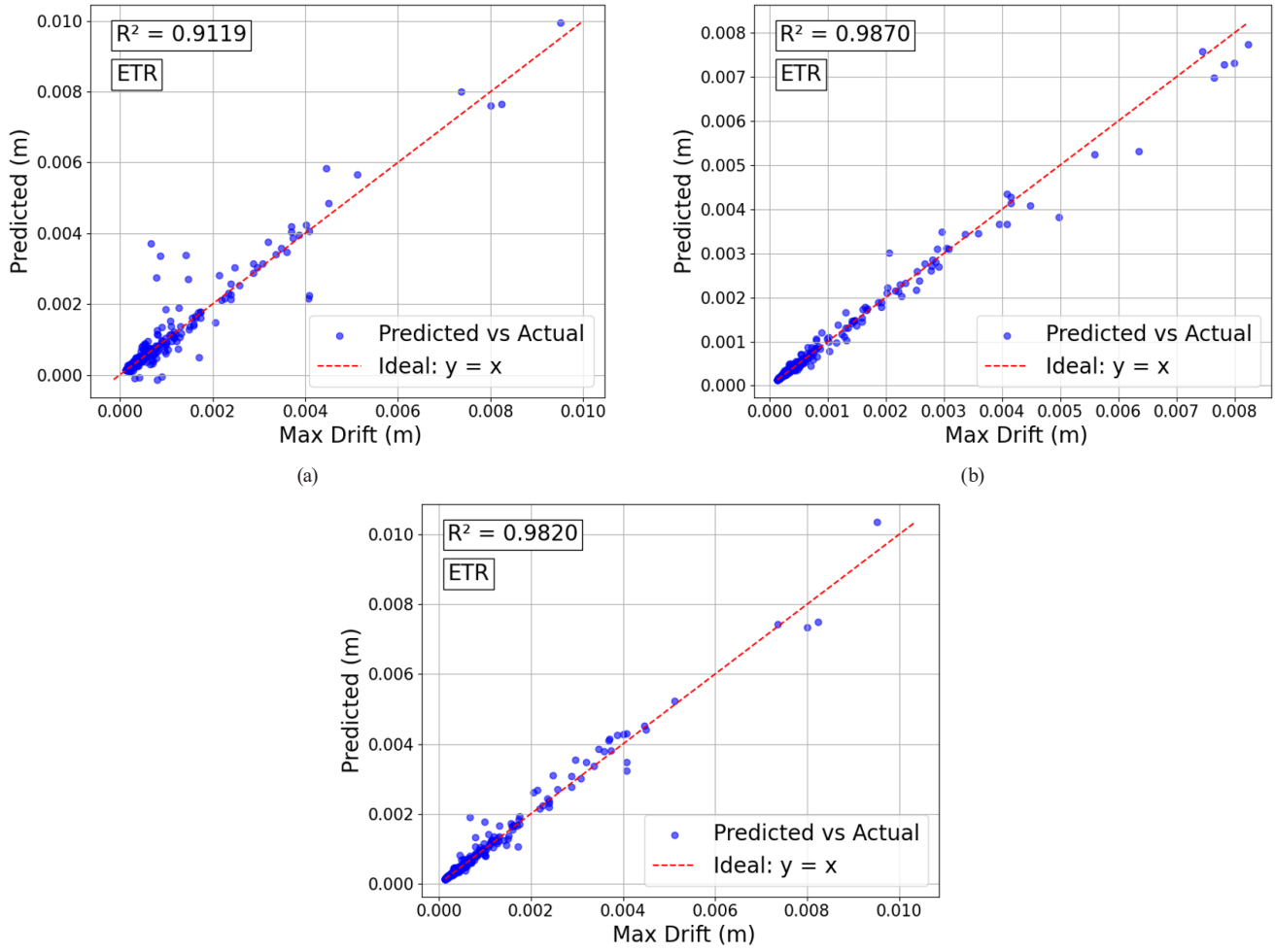

Fig. 6 Maximum drift prediction of (a) 4 story, (b) 8 story, (c) 12 story

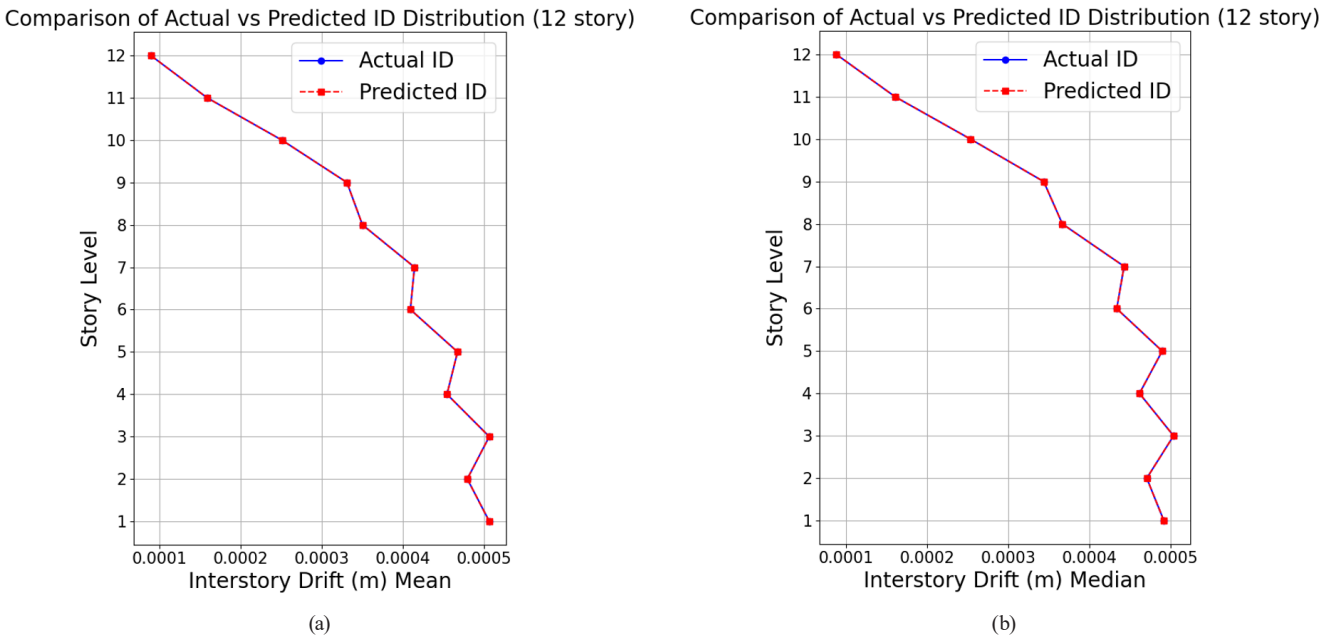

Fig. 7 Predictions of the ID distribution for 4 story using the proposed Stacked ML-based model assuming the (a) mean (b) median methods

Table 9 and Table 10 provide error metrics for the inter-story drift distribution of a 12-story, 3D reinforced concrete building using the median and mean methods, respectively. Tables 9 and 10 show that the stacked ML model achieves the highest R^2 values and lowest error metrics, confirming its superior performance. To assess efficiency, we measured the execution times of all models (see Tables 9 and 10). The stacked model, while highly accurate, has the longest runtime due to its use of multiple base estimators and result aggregation.

For a complete picture, error metrics for the inter-story drift distribution of 4- and 8-story buildings using both mean and median methods are provided in Tables A1–A4 in the Appendix. To make the results easier to understand, we visualized the performance of various ML methods from Tables 9, 10, and A1–A4 in charts. Fig. 8 shows each algorithm's performance based on error metrics using the mean, with ETR and RF standing out for their high R^2 values. The stacked model, combining multiple algorithms, achieves the highest R^2 and lowest errors across all metrics, while maintaining efficient runtime. Fig. 9, using the median method, further confirms the stacked model's reliability and effectiveness. These visualizations provide designers with clear, accurate, and practical insights for optimizing structural designs. To express the predictive accuracy in engineering terms, the mean absolute error for drift predictions corresponds to approximately 0.006–0.012 drift ratio (≈2–8 mm of lateral displacement for typical 8–12 story buildings), representing 10–20% relative error for moderate-to-high intensity cases. These values are significantly smaller than the drift thresholds commonly used in performance-based design (1–3%), indicating that the ML models provide accuracy that is appropriate for engineering decision-making.

5 Conclusions

This study employs machine learning (ML) to predict the seismic responses of 3D reinforced concrete (RC) buildings, enabling rapid and accurate guidance for optimal structural design. Buildings were modeled using OpenSees software [37] and subjected to nonlinear time-history analyses under 110 far-field earthquake records from the PEER database, evaluating inter-story drift (ID), maximum drift (MD) and roof drift (RD).

Sensitivity analysis reduced 21 initial input parameters to 10 key features: seismic inputs (PGA, PGV, PGD, AI, ASI, HI, SD) and structural inputs (number of floors, total height, width). The most influential factors were building height, width, HI, and ASI.

Ten ML algorithms were assessed, with Extra Trees Regressor (ETR), Random Forest (RF), Gradient Boosting Regression (GBR), and XGBoost showing superior performance for predicting maximum structural drift, inter-story drift, and roof drift using mean and median methods. For 4-story structures, R^2 values were 0.9388 (ETR), 0.9289 (RF), and 0.9226 (GBR); for 8-story, 0.9833 (RF),

Table 9 Result of error of indicator for the ID distribution of 12 story RC frame assuming mean method

ML algorithm	*R*-squared	MSE	MAE	MARE	MSRE	RMSRE
RF	0.9622	7.05E-10	1.23E-05	0.0362	0.003318	0.057599
XGBoost	0.9447	1.80E-09	1.58E-05	0.0328	0.00283	0.053198
ETR	0.9798	9.33E-10	1.80E-05	0.0318	0.002217	0.047087
GBR	0.9827	8.19E-10	1.65E-05	0.0291	0.00175	0.04183
HGBR	0.9665	1.15E-09	1.53E-05	0.0333	0.002327	0.048237
LightGBM	0.9435	1.62E-10	5.64E-06	0.0475	0.00605	0.077781
Stacked ML	0.9996	9.15E-10	1.76E-05	0.0288	0.001733	0.041633

Table 10 Result of error of indicator for the ID distribution of 12 story RC frame assuming median method

ML algorithm	*R*-squared	MSE	MAE	MARE	MSRE	RMSRE
RF	0.9534	4.78E-10	8.95E-06	0.0393	0.004358	0.066015
XGBoost	0.9305	1.30E-09	1.31E-05	0.0347	0.003337	0.057765
ETR	0.9764	9.93E-10	1.77E-05	0.033	0.002386	0.048845
GBR	0.983	7.17E-10	1.51E-05	0.00281	0.001612	0.040151
HGBR	0.9529	8.79E-10	1.39E-05	0.0407	0.003989	0.063156
LightGBM	0.9374	6.42E-10	1.06E-05	0.0465	0.005775	0.07599
Stacked ML	0.9995	1.03E-09	1.81E-05	0.031	0.002026	0.045006

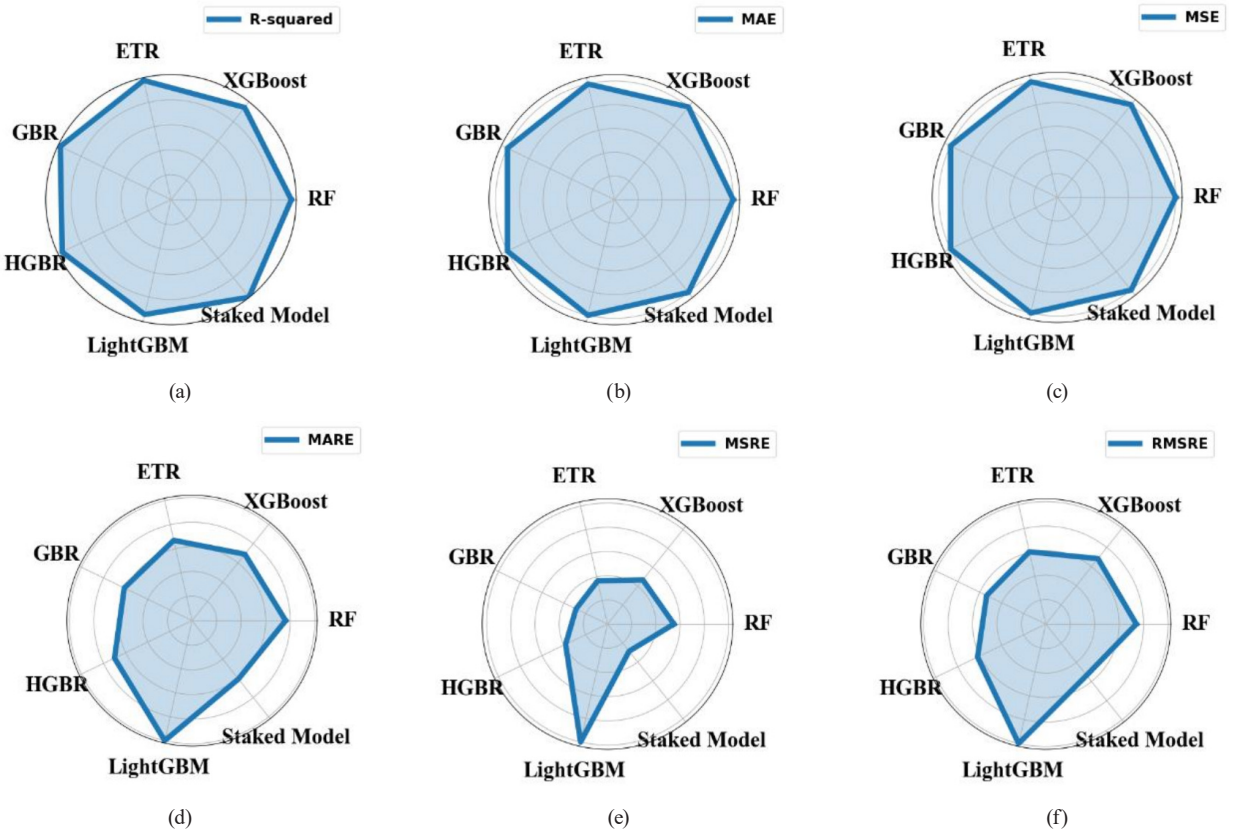

Fig. 8 Prediction results using ML methods on a 12-story building using (a) *R*-squared, (b) MAE, (c) MSE, (d) MARE, (e) MSRE, and (f) RMSRE error measures with the mean method

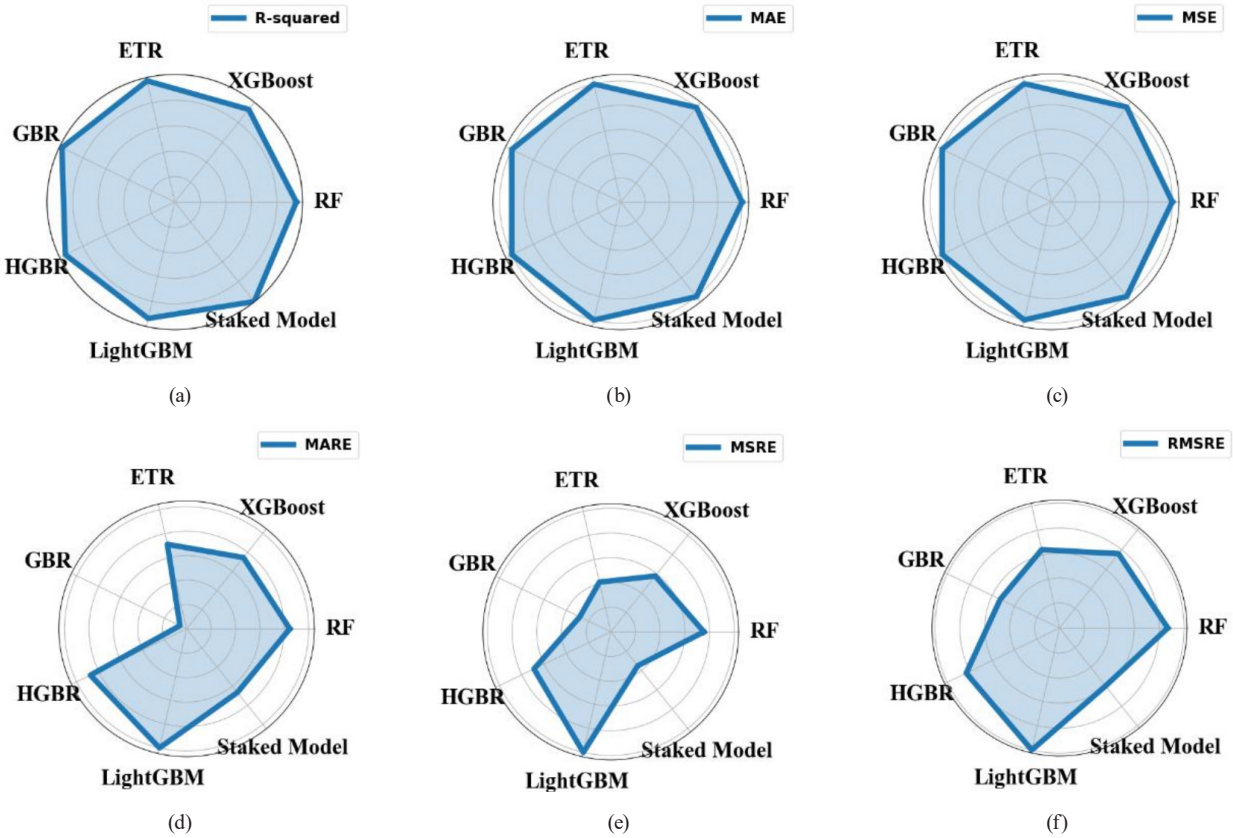

Fig. 9 Prediction results using ML methods on a 12-story building using (a) *R*-squared, (b) MAE, (c) MSE, (d) MARE, (e) MSRE, and (f) RMSRE error measures with the median method

0.9787 (GBR), and 0.9781 (ETR); for 12-story, 0.9827 (GBR), 0.9798 (ETR), and 0.9622 (RF). ETR excelled for 4-story buildings, RF for 8-story, and GBR for 12-story. Across all structures for maximum drift, R^2 values were 0.9684 (XGBoost), 0.9678 (ETR), and 0.9612 (RF).

To improve accuracy, generalizability, and efficiency, a stacked ensemble model combining ETR, RF, and XGBoost was developed, incorporating parallel processing. It achieved R^2 of 0.9957 for maximum drift prediction, 0.9886–0.9996 for inter-story drift across structures, exceeding 0.99 for 12-story buildings and 0.95 for 4- and 8-story, with >99.9% accuracy for inter-story drift distribution in 3D RC structures.

This approach facilitates performance-based seismic design by enabling designers to optimize resilience, identify vulnerabilities (e.g., soft stories), and develop efficient structures. Although some records produced very low drift responses, the use of absolute error metrics ensured stable evaluation, and additional checks confirmed that model performance and ranking were not affected by the presence of low-intensity cases.

References

[1] Todorov, B., Muntasir Billah, A. H. M. "Post-earthquake seismic capacity estimation of reinforced concrete bridge piers using Machine learning techniques", Structures, 41, pp. 1190–1206, 2022. https://doi.org/10.1016/j.istruc.2022.05.067

[2] Ramesh, V., Anbarasan, M. I., Muthuramu, B. "Advanced strategies in earthquake-resistant structural engineering: seismic design, materials, and innovations", Asian Journal of Civil Engineering, 26(4), pp. 1413–1428, 2025. https://doi.org/10.1007/s42107-025-01298-8

[3] Yön, B., Dedeoğlu, İ. Ö., Yetkin, M., Erkek, H., Calayır, Y. "Evaluation of the seismic response of reinforced concrete buildings in the light of lessons learned from the February 6, 2023, Kahramanmaraş, Türkiye earthquake sequences", Natural Hazards, 121(1), pp. 873–909, 2025. https://doi.org/10.1007/s11069-024-06859-9

[4] Onat, O., Tanyıldızı, H. "Machine learning-based estimation of the out-of-plane displacement of brick infill exposed to earthquake shaking", Engineering Applications of Artificial Intelligence, 136, 109007, 2024. https://doi.org/10.1016/j.engappai.2024.109007

[5] Afzal, M., Liu, Y., Cheng, J. C. P., Gan, V. J. L. "Reinforced concrete structural design optimization: A critical review", Journal of Clean Production, 260, 120623, 2020. https://doi.org/10.1016/j.jclepro.2020.120623

[6] Latif, I., Surana, M., Banerjee, A. "Effects of material properties uncertainty on seismic fragility of reinforced-concrete frames using machine learning approach", Journal of Building Engineering, 86, 108871, 2024. https://doi.org/10.1016/j.jobe.2024.108871

[7] Liu, R., Yang, Y. "Experimental study on seismic performance of seismic-damaged RC frame retrofitted by prestressed steel strips", Bulletin of Earthquake Engineering, 18(14), pp. 6475–6486, 2020. https://doi.org/10.1007/s10518-020-00931-y

[8] Cheng, Q., Li, A., Ren, H., Chea, C. P., Liao, W., Xie, L. "Rapid seismic-damage assessment method for buildings on a regional scale based on spectrum-compatible data augmentation and deep learning", Soil Dynamics and Earthquake Engineering, 178, 108504, 2024. https://doi.org/10.1016/j.soildyn.2024.108504

[9] Hashmi, A. K., Singh, H. K., Jameel, M., Patil L. G. "Performance-based efficient seismic design of reinforced concrete frames with vertical irregularities", Asian Journal of Civil Engineering, 23(3), pp. 375–389, 2022. https://doi.org/10.1007/s42107-022-00429-9

[10] Moghaddam, H., Hajirasouliha, I., Hosseini Gelekolai, S. M. "Performance-based seismic design of moment resisting steel frames: Adaptive optimisation framework and optimum design load pattern", Structures, 33, pp. 1690–1704, 2021. https://doi.org/10.1016/j.istruc.2021.05.014

[11] Cheng, S., Han, J., Shang, J. "Optimal repair decision and seismic resilience analysis of seismic-damaged RC structures considering rebar corrosion", Journal of Building Engineering, 112, 113749, 2025. https://doi.org/10.1016/j.jobe.2025.113749

[12] Demir, A., Sahin E. K., Demir, S. "Advanced tree-based machine learning methods for predicting the seismic response of regular and irregular RC frames", Structures, 64, 106524, 2024. https://doi.org/10.1016/j.istruc.2024.106524

[13] Luo, H., Paal, S. G. "Artificial intelligence-enhanced seismic response prediction of reinforced concrete frames", Advances in Engineering Informtics, 52, 101568, 2022. https://doi.org/10.1016/j.aei.2022.101568

[14] Bhatta, S., Kang, X., Dang, J. "Machine learning prediction models for ground motion parameters and seismic damage assessment of buildings at a regional scale", Resilient Cities and Structures, 3(1), pp. 84–102, 2024. https://doi.org/10.1016/j.rcns.2024.03.001

[15] Aloisio, A., Santis, Y. D., Irti, F., Pasca, D. P., Scimia, L., Fragiacomo, M. "Machine learning predictions of code-based seismic vulnerability for reinforced concrete and masonry buildings: Insights from a 300-building database", Engineering Structures, 301, 117295, 2024. https://doi.org/10.1016/j.engstruct.2023.117295

[16] Nica, G.-B., Pavel, F., Hojda, G. "A fast nonlinear dynamic analysis automated approach to produce fragility curves for 3D RC frames", Engineering Structures, 281, 115695, 2023. https://doi.org/10.1016/j.engstruct.2023.115695

[17] Pak, H., Paal, S. G. "A real-time structural seismic response prediction framework based on transfer learning and unsupervised learning", Engineering Structures, 323, 119227, 2025. https://doi.org/10.1016/j.engstruct.2024.119227

[18] Feng, D.-C., Chen, S.-Z., Taciroglu, E. "Deep learning-enhanced efficient seismic analysis of structures with multi-fidelity modeling strategies", Computer Methods in Applied Mechanics and Engineering, 421, 116775, 2024. https://doi.org/10.1016/j.cma.2024.116775

[19] Azarhoosh, Z., Ilchi Ghazaan, M. "A review of recent advances in surrogate models for uncertainty quantification of high-dimensional engineering applications", Computer Methods in Applied Mechanics and Engineering, 433, 117508, 2025. https://doi.org/10.1016/j.cma.2024.117508

[20] Gondaliya, K. M., Vasanwala, S. A., Desai, A. K., Amin, J. A., Bhaiya, V. "Machine learning-based approach for assessing the seismic vulnerability of reinforced concrete frame buildings", Journal of Building Engineering, 97, 110785, 2024. https://doi.org/10.1016/j.jobe.2024.110785

[21] Hwang, S.-H., Mangalathu, S., Shin, J., Jeon, J.-S. "Machine learning-based approaches for seismic demand and collapse of ductile reinforced concrete building frames", Journal of Building Engineering, 34, 101905, 2021. https://doi.org/10.1016/j.jobe.2020.101905

[22] Habib, A., Junaid, M. T., Dirar, S., Barakat, S., Al-Sadoon, Z. A. "Machine Learning-Based Estimation of Reinforced Concrete Columns Stiffness Modifiers for Improved Accuracy in Linear Response History Analysis", Journal of Earthquake Engineering, 29(1), pp. 130–155, 2025. https://doi.org/10.1080/13632469.2024.2409865

[23] Jagruthi, N., Sharathchandran, K., Pandikkadavath, M. S., Mangalathu, S., Reddy, K. M., Nair, A., Sahoo, D. R. "Machine Learning-Based Seismic Drift Response Estimation of Buckling-Restrained Braced Frames", In: Proceedings of 17th Symposium on Earthquake Engineering (Vol. 2), Roorkee, India, 2023, pp. 837–848. ISBN 978-981-99-1603-0 https://doi.org/10.1007/978-981-99-1604-7_63

[24] Kaveh, A. "Applications of Artificial Neural Networks and Machine Learning in Civil Engineering", Springer, 2024. ISBN 978-3-031-66050-4 https://doi.org/10.1007/978-3-031-66051-1

[25] Zhang, T., Xu, W., Wang, S., Du, D., Tang, J. "Seismic response prediction of a damped structure based on data-driven machine learning methods", Engineering Structures, 301, 117264, 2024. https://doi.org/10.1016/j.engstruct.2023.117264

[26] Bhatta, S., Dang, J. "Seismic damage prediction of RC buildings using machine learning", Earthquake Engineering & Structural Dynamics, 52(11), pp. 3504–3527, 2023. https://doi.org/10.1002/eqe.3907

[27] Xu, Y., Li, Y., Zheng, X., Zheng, X., Zhang, Q. "Computer-Vision and Machine-Learning-Based Seismic Damage Assessment of Reinforced Concrete Structures, Buildings, 13(5), 1258, 2023. https://doi.org/10.3390/buildings13051258

[28] Shafaie, V., Movahedi Rad, M. "Dem-driven investigation and AutoML-Enhanced prediction of Macroscopic behavior in cementitious composites with Variable frictional parameters", Materials & Design, 254, 114069, 2025. https://doi.org/10.1016/j.matdes.2025.114069

[29] Ahmed, B., Mangalathu, S., Jeon J.-S. "Seismic damage state predictions of reinforced concrete structures using stacked long short-term memory neural networks", Journal of Building Engineering, 46, 103737, 2022. https://doi.org/10.1016/j.jobe.2021.103737

[30] Lazaridis, P. C., Kavvadias, I. E., Demertzis, K., Iliadis, L., Vasiliadis, L. K. "Interpretable machine learning for assessing the cumulative damage of a reinforced concrete frame induced by seismic sequences", [preprint] Preprints.org, 10 May 2023. Available at: https://www.preprints.org/manuscript/202305.0737/v1

[31] Kaveh, A., Ilchi Ghazaan, M. "Optimum seismic design of 3D irregular steel frames using recently developed metaheuristic algorithms", Journal of Computing in Civil Engineering, 32(3), 04018015, 2018. https://doi.org/10.1061/(ASCE)CP.1943-5487.0000760

[32] Zhang, H., Cheng, X., Li, Y., He, D., Du, X. "Rapid seismic damage state assessment of RC frames using machine learning methods", Journal of Building Engineering, 65, 105797, 2023. https://doi.org/10.1016/j.jobe.2022.105797

[33] Shafaie, V., Ghodousian, O., Ghodousian, A., Homayounfar, M., Movahedi Rad, M. "Slant shear tests and fuzzy logic integration for evaluating shear bond strength in SCC and FRSCC repair applications", Case Studies in Construction Materials, 22, e04176, 2025. https://doi.org/10.1016/j.cscm.2024.e04176

[34] Shafaie, V., Movahedi Rad, M. "Multi-objective genetic algorithm calibration of colored self-compacting concrete using DEM: An integrated parallel approach", Scientific Reports, 14(1), 4126, 2024. https://doi.org/10.1038/s41598-024-54715-4

[35] Samadian, D., Muhit, I. B., Occhipinti, A., Dawood, N. "Meta databases of steel frame buildings for surrogate modelling and machine learning-based feature importance analysis", Resilient Cities and Structures, 3(1), pp. 20–43, 2024. https://doi.org/10.1016/j.rcns.2023.12.001

[36] CSI "ETABS V16.1.1, Integrated software for structural analysis and design", [computer program] Computers and Structures Inc., Walnut Creek, CA, USA, 2016.

[37] McKenna, F., Scott, M. H., Fenves, G. L. "Nonlinear finite-element analysis software architecture using object composition", Journal of Computing in Civil Engineering, 24(1), pp. 95–107, 2010. https://doi.org/10.1061/(ASCE)CP.1943-5487.0000002

[38] ASCE "ASCE/SEI 7-16 Minimum design loads and associated criteria for buildings and other structures", American Society of Civil Engineers, Reston, VA, USA, 2017. https://doi.org/10.1061/9780784414248

[39] ACI Committee 318 "318-14: Building Code Requirements for Structural Concrete and Commentary", American Concrete Institute, 2014. https://doi.org/10.14359/51688187

[40] ASCE "ASCE/SEI 41-17 Seismic Evaluation and Retrofit of Existing Buildings", American Society of Civil Engineers, Reston, VA, USA, 2017. https://doi.org/10.1061/9780784414859

[41] Sen, A., Cook, D., Liel, A., Basnet, T., Creagh, A., …, Smith, R. "ASCE/SEI 41 assessment of reinforced concrete buildings: Benchmarking linear procedures and FEMA P-2018 with empirical damage observations", Earthquake Spectra, 39(3), pp. 1658–1682, 2023. https://doi.org/10.1177/87552930231173454

[42] Lazaridis, P. C., Kavvadias, I. E., Demertzis, K., Iliadis, L., Vasiliadis, L. K. "Structural damage prediction of a reinforced concrete frame under single and multiple seismic events using machine learning algorithms", Applied Sciences, 12(8), 3845, 2022. https://doi.org/10.3390/app12083845

[43] Shehzad, A., Xiu-Xin, W., Xing-Huai, H., Ullah, K., Mohammad, A., Althobaiti, A., Flah, A. "AI-driven seismic optimization of outrigger systems in high-rise buildings: A machine learning framework for enhanced performance in earthquake-prone regions", Journal of Building Engineering, 112, 113864, 2025. https://doi.org/10.1016/j.jobe.2025.113864

[44] Enginler, S. Ö., Küçükdeniz, T., Dal, G. E., Yıldırım, F., Cilasun, G. E., …, Karakuş, S. "Enhancing electrochemical detection through machine learning-driven prediction for canine mammary tumor biomarker with green silver nanoparticles", Analytical and Bioanalytical Chemistry, 416(23), pp. 5071–5088, 2024. https://doi.org/10.1007/s00216-024-05444-0

[45] Demirtaş, B., Türker, T., Yanik, Y., Dede, T. "Frequency-Based Damage Detection with ANN and Seismic Behaviour Assessment of a Historical Masonry Tower", Iranian Journal of Science and Technology, Transactions of Civil Engineering, 2025. https://doi.org/10.1007/s40996-025-01816-3

[46] Deniz, E. "Evaluating the effectiveness of machine learning models in predicting student academic achievement", ADBA Computer Science, 1(1), pp. 8–13, 2024. https://doi.org/10.69882/adba.cs.2024072

[47] Das, A., Asieb Hasan, K. M. "Leveraging meteorological data and machine learning for improved rainfall forecasting in Australia", In: 2024 IEEE International Conference on Internet of Things and Intelligence Systems (IoTaIS), Bali, Indonesia, 2024, pp. 265–269. ISBN 979-8-3315-2122-6 https://doi.org/10.1109/IoTaIS64014.2024.10799343

[48] Galveias, A., Antunes, C., Costa, A. R., Fraga, H. "Pollen- and Weather-Based Machine Learning Models for Estimating Regional Olive Production", Horticulturae, 10(6), 584, 2024. https://doi.org/10.3390/horticulturae10060584

[49] Suenaga, D., Takase, Y., Abe, T., Orita, G., Ando, S. "Prediction accuracy of Random Forest, XGBoost, LightGBM, and artificial neural network for shear resistance of post-installed anchors", Structures, 50, pp. 1252–1263, 2023. https://doi.org/10.1016/j.istruc.2023.02.066

[50] Tang, Q., Cui, Y., Jia, J. "Machine learning-based surrogate resilience modeling for preliminary seismic design", Journal of Building Engineering, 98, 111226, 2024. https://doi.org/10.1016/j.jobe.2024.111226

[51] Chitkeshwar, A. "Revolutionizing Structural Engineering: Applications of Machine Learning for Enhanced Performance and Safety", Archives of Computational Methods in Engineering, 31(8), pp. 4617–4632, 2024. https://doi.org/10.1007/s11831-024-10117-3

[52] Gong, C., Liu, J., Dai, S., Hao, H., Liu, H. "Machine learning assisted prediction of the phonon cutoff frequency of ABO_3 perovskite materials", Computational Material Sciences, 239, 112943, 2024. https://doi.org/10.1016/j.commatsci.2024.112943

[53] Hathal, M. S., Saeed, B. M., Abdulqader, D. A., Mustafa, F. M. "Attack and anomaly prediction in networks-on-chip of multiprocessor system-on-chip-based IoT utilizing machine learning approaches", Service Oriented Computing and Applications, 18(3), pp. 209–223, 2024. https://doi.org/10.1007/s11761-024-00393-z

[54] Kazemi, F., Asgarkhani, N., Jankowski, R. "Machine learning-based seismic response and performance assessment of reinforced concrete buildings", Archives of Civil and Mechanical Engineering, 23(2), 94, 2023. https://doi.org/10.1007/s43452-023-00631-9

Appendix

Results of error for the considered frames are provided in Tables A1–A4.

Table A1 Result of error indicator for the ID distribution of 4 story RC frame assuming mean method

ML algorithm	*R*-squared	MSE	MAE	MARE	MSRE	RMSRE
RF	0.9289	3.93E-08	4.96E-05	0.0733	0.019259	0.138776
XGBoost	0.8711	1.94E-09	2.62E-05	0.3204	0.136383	0.3693
ETR	0.9388	1.44E-10	4.61E-06	0.0429	0.004654	0.068219
GBR	0.9226	1.55E-09	1.18E-05	0.0498	0.00873	0.093436
HGBR	0.9149	1.53E-10	5.23E-06	0.0484	0.005877	0.076664
LightGBM	0.9189	1.30E-09	1.28E-05	0.0599	0.010546	0.102695
Stacked ML	0.9886	1.24E-08	4.69E-06	0.03985022	0.00428232	0.06543943

Table A2 Result of error indicator for the ID distribution of 4 story RC frame assuming median method

ML algorithm	*R*-squared	MSE	MAE	MARE	MSRE	RMSRE
RF	0.9273	2.04E-10	5.26E-06	0.0452	0.006131	0.078302
XGBoost	0.8926	1.84E-09	3.07E-05	0.2333	0.077612	0.278588
ETR	0.9375	1.36E-09	1.15E-05	0.0498	0.008627	0.092883
GBR	0.9268	1.52E-10	4.74E-06	0.0424	0.004514	0.067184
HGBR	0.9018	4.88E-08	7.59E-05	0.1704	0.064793	0.254545
LightGBM	0.9174	3.86E-08	6.46E-05	0.1594	0.054907	0.234323
Stacked ML	0.9862	2.57E-08	1.2E-05	0.04890834	0.00903359	0.09504522

Table A3 Result of error indicator for the ID distribution of 8 story RC frame assuming mean method

ML algorithm	*R*-squared	MSE	MAE	MARE	MSRE	RMSRE
RF	0.9781	6.91E-08	8.05E-05	0.1247	0.964757	0.98222
XGBoost	0.9656	7.67E-08	1.32E-04	0.4964	0.446023	0.667849
ETR	0.9833	1.86E-08	4.89E-05	0.0512	0.010188	0.100934
GBR	0.9787	3.56E-08	8.97E-05	0.3722	0.012101	0.110005
HGBR	0.9082	5.09E-09	2.52E-05	0.1076	0.025987	0.161206
LightGBM	0.9145	7.40E-09	3.82E-05	0.1038	0.030515	0.174685
Stacked ML	0.9994	1.86E-08	4.89E-05	0.0512	0.010188	0.100934

Table A4 Result of error indicator for the ID distribution of 8 story RC frame assuming median method

ML algorithm	*R*-squared	MSE	MAE	MARE	MSRE	RMSRE
RF	0.9775	3.57E-09	1.86E-05	0.0615	0.012053	0.109786
XGBoost	0.9652	1.02E-08	6.38E-05	0.2821	0.112163	0.334908
ETR	0.9827	6.30E-09	1.74E-05	0.0496	0.00758	0.087062
GBR	0.9799	2.27E-09	2.58E-05	0.0779	0.013295	0.115305
HGBR	0.9025	5.35E-09	3.38E-05	0.1291	0.042073	0.205118
LightGBM	0.9137	9.95E-09	4.62E-05	0.1246	0.039459	0.198643
Stacked ML	0.9992	6.30E-09	1.74E-05	0.0496	0.00758	0.087062